LA-UR-04-1899
Approved for public release;
distribution is unlimited.

March 15, 2004

Title: Constitutive model for PMMA at high pressure

Author(s): Ralph Menikoff, rtm@lanl.gov

Submitted to: Journal of Applied Physics

Constitutive model for PMMA at high pressure

Ralph Menikoff*
Los Alamos National Laboratory
Los Alamos, New Mexico 87545
(Dated: March 15, 2004)

A constitutive model of PMMA is developed for use in analyzing VISAR experiments that utilize PMMA as a window material. A thermodynamically consistent, fully three dimensional rate dependent elastic-plastic model is calibrated to data for (i) shock speed, (ii) release wave speed behind shock, (iii) shear stress behind shock, (iv) shear wave speed from static compression and (v) shock wave profiles. The model is intended for the regime of shock experiments; microsecond time scale and stress up to 10 GPa.

PACS numbers: 62.20.Fe, 62.50.+p, 64.30.+t
Keywords: PMMA, shock wave profiles, EOS

I. INTRODUCTION

PMMA[1] remains transparent under shock compression, and is used as a window material for VISAR[2] experiments. These experiments measure a velocity time history at the sample/window interface during the passage of a high pressure compression wave, often referred to as shock wave, even though strictly speaking, a shock is a discontinuity. In order to infer the response of the sample (*i.e.,* wave profile) from the VISAR record, the response of the window material is needed to account for the impedance mismatch of a wave at the sample/window interface.

Many experiments have been performed to characterize the material response of PMMA. These include the following:

1. Ultrasonic measurements of the longitudinal and transverse acoustic speeds under static compression up to 1 GPa [2, 3].

2. Measurements of the principal shock Hugoniot [4–6]. These experiments determined the shock pressure as a function of compression, and measured wave profiles after various lengths of propagation. In addition, the release wave speed, which corresponds to the longitudinal sound speed behind the shock front, was measured.

3. Shear stress behind the shock wave [7–12]. Gupta [7] used an oblique impact to generate a shear wave and measured its wave speed. The other experiments used piezoresistive foil gauges (either Manganin, ytterbium or carbon) to measure the shear stress behind a longitudinal wave. It is important to note that the data from early experiments, such as [8], are incorrect because the response of the piezoresistive element to its anisotropic surroundings and therefore its calibration in the shear mode were not understood at the time the experiments were performed. Results from the most recent experiments [10, 12] are consistent.

4. Thermal properties such as the temperature dependence of the shear modulus [13] and specific heat [14] at atmospheric pressure, and the temperature as a function of pressure along isentropes [15, 16] and the principal shock Hugoniot [17]. We note that at atmospheric pressure the glass transition temperature is 378 K. At the glass transition, the specific heat increases by 20 % and the static shear modulus decreases by three orders of magnitude. The stress dependence of the glass transition temperature has not been measured.

The shock wave profiles show a strong relaxation response. Since PMMA is a polymer, viscoelastic models have been used to describe its response, see for example [6, Sec. 3]. However, viscoelastic models typically are applicable at lower pressures and longer time scales than occurs in shock wave experiments. Moreover, PMMA exhibits a yield behavior that depends on pressure, temperature and strain rate [18, 19]. Elastic-plastic models have also been used [20]. These models include strain rate, thermal softening and strain hardening effects but do not include compressible effects needed for shock waves.

Yet the PMMA wave profiles can be viewed as displaying the qualitative features associated with a rate dependent elastic-plastic model. These include a partly dispersed wave profile (discontinuous shock followed by relaxation layer) and transient wave profile approaching steady state with increasing distance of run. A distinctive aspect of elastic-plastic waves that is not displayed

*Electronic address: rtm@lanl.gov
[1] Polymethyl methacrylate, also known under the trade names plexiglass and lucite. The properties of a polymer vary somewhat with the manufacturing process. The shock experiments of most interest in this paper used Rohm and Haas type II UVA plexiglass.
[2] Velocity Interferometry System for Any Reflector, for a review of the technique see [1].

by PMMA is a two-wave structure; elastic-precursor followed by plastic wave. However, the Hugoniot locus in the (particle-velocity,shock-velocity)–plane displays a rapid change in slope around 0.7 GPa. Rosenberg & Partom [21] associated this with the Hugoniot elastic limit, and proposed a pressure dependent yield strength to reconcile difference with static strength. A similar idea is used here. By choosing a yield strength to increase with compression, no split waves occur and the wave profiles are always partly dispersed.

The aim of this paper is to construct a thermodynamically consistent rate dependent elastic-plastic model for PMMA that can account for the tensorial nature of the stress (three-dimensional model), for the non-linearities in the shear strain, and for the relaxation in shock wave profiles. The non-linearities are important because the elastic shear strain behind the discontinuity in a partly dispersed wave is large enough to be outside the linear regime. We also note that rate-dependent plasticity reduces to a viscoelastic model in the limit of slow strain rates. The emphasis here is on the large strain rates ($\sim 10^6$ per second) that occur in shock profiles.

The remainder of this paper is organized as follows. Section 2 describes the hyper-elastic model that is used. Shock experiments correspond to uniaxial strain. Uniaxial strain greatly simplifies the model. The reduction to the 1-dimensional model is presented in section 3. Experimental data and calibration of the model for PMMA is described in section 4. We note that the yield strength and the shear modulus determine the plastic strain on the yield surface. To calibrate the model it is more convenient to fit the plastic strain to the acoustic speed on the Hugoniot locus, and then use the yield strength, *i.e.,* shear stress, as a consistency check. Wave profiles and the plastic relaxation are presented in section 5.

II. HYPER-ELASTIC MODEL

A hyper-elastic model is defined by the specific energy. We consider an isotropic material and assume that the energy is the sum of hydrostatic and shear components of the form

$$\mathcal{E}(\mathbf{C}, \mathbf{C_p}, S) = \mathcal{E}_{\rm hydro}(V, S) + \mathcal{E}_{\rm shear}(V, I_1, I_2) \ ,$$

where V is specific volume, $\mathbf{C} = \mathbf{F}^T\mathbf{F}$ is the right Cauchy-Green tensor, $\mathbf{F}$ is the deformation gradient, $\mathbf{C_p}$ is the plastic analog of $\mathbf{C}$, S is the entropy, I_j are the invariants of $\mathbf{b}_{\rm el} = \mathsf{J}^{-2/3}\,{\mathbf{C_p}}^{-1}\mathbf{C}$, and $\mathsf{J} = V/V_0$. The invariants are

$$\begin{aligned} I_1 &= \mathsf{Tr}\,(\mathbf{b}_{\rm el}) \ , \\ I_2 &= \tfrac{1}{2}\Big(I_1^2 - \mathsf{Tr}\,({\mathbf{b}_{\rm el}}^2)\Big) \ , \end{aligned}$$

and assuming $\mathsf{det}\,\mathbf{C_p} = 1$, $I_3 = 1$. In effect, $\mathbf{C_p}$ plays the role of a metric, and $\frac{1}{2}(\mathbf{b}_{\rm el} - \mathbf{I})$ is used as a measure of the elastic shear strain since $\mathbf{b}_{\rm el}$ is scaled to be independent of hydrostatic compression.

For simplicity, we further assume that the shear energy has the form

$$\mathcal{E}_{\rm shear} = \tfrac{1}{2}\,V\,G(V)\Big[\mathsf{Tr}\,(\mathbf{b}_{\rm el}) - 3\Big] \ ,$$

where $G(V)$ is shown below to correspond to the hydrostatic shear modulus. The Cauchy stress splits naturally into hydrostatic and deviatoric components

$$\begin{aligned} \boldsymbol{\sigma} &= 2\,\mathsf{J}^{-1}\,\mathbf{F}\,\frac{\partial \mathcal{E}}{\partial \mathbf{C}}\,\mathbf{F}^T \\ &= -P\,\mathbf{I} + 2\,G(V)\ \mathsf{dev}\,(\mathbf{b}_{\rm el}) \ , \end{aligned}$$

where the pressure is

$$P = P_{\rm hydro}(V, S) + P_{\rm shear}(V, \mathbf{b}_{\rm el}) \ ,$$

with hydrostatic and shear components

$$\begin{aligned} P_{\rm hydro} &= -\Big(\frac{\partial}{\partial V}\mathcal{E}_{\rm hydro}\Big)_S \ , \\ P_{\rm shear} &= -\tfrac{1}{2}\frac{d}{dV}\Big(V\,G\Big)\Big[\mathsf{Tr}\,(\mathbf{b}_{\rm el}) - 3\Big] \ . \end{aligned}$$

To compare with data we need the acoustic speeds, both longitudinal and transverse. These are determined by the acoustic tensor. For a wave propagating in the $\hat{n}$-direction the wave speeds, actually $\rho\,c^2$, are the eigenvalues of the matrix $\overline{\mathbf{a}}(\hat{n})$ with components

$$\begin{aligned} \overline{\mathsf{a}}(\hat{n})^{ij} = A_1\,n^i n^j + A_2\,\Big(n^i[\mathsf{dev}\,(\mathbf{b}_{\rm el})\,\hat{n}]^j + n^j[\mathsf{dev}\,(\mathbf{b}_{\rm el})\,\hat{n}]^i\Big) \\ + A_3\,\delta^{ij} \ , \end{aligned}$$

where

$$\begin{aligned} A_1 = \ & \rho\,c^2_{\rm hydro} + \tfrac{1}{9}\ \mathsf{Tr}\,(\mathbf{b}_{\rm el})\ G \\ & + \mathsf{J}\Big[\mathsf{Tr}\,(\mathbf{b}_{\rm el}) - 3\Big]\Big[V\frac{d}{dV}G + \tfrac{1}{2}V^2\Big(\frac{d^2}{dV^2}\Big)G\Big] \ , \end{aligned}$$

$$A_2 = \tfrac{1}{3}\,G + V\frac{d}{dV}G \ ,$$

$$A_3 = (\hat{n},\,\mathbf{b}_{\rm el}\,\hat{n})\,G \ ,$$

$$c^2_{\rm hydro} = -V^2\Big(\frac{\partial}{\partial V}P_{\rm hydro}\Big)_S \ .$$

For hydrostatic compression, $(\mathbf{b}_{\rm el})^{ij} = \delta^{ij}$, and the acoustic speeds are

$$\begin{aligned} \rho\,c^2_{\rm long} &= \rho\,c^2_{\rm hydro} + \tfrac{4}{3}\,G(V) \ , \\ \rho\,c^2_{\rm tran} &= G(V) \ . \end{aligned}$$

Thus, $G(V)$ corresponds to the hydrostatic shear modulus.

The model described is thermodynamically consistent and fully three dimensional. The main limitations of the model are the neglect of the temperature dependence of

the shear modulus and the assumption that $\det \mathbf{C_p} = 1$. The model can be extended to include thermal effects [22]. The limited data available on the temperature dependence of the shear modulus is from acoustic measurements; up to 75 C at 6 Mhz [2, fig. 5] and up to 200 C at 1 Hz [13, figs. 8 and 12], both at atmospheric pressure. We note that the sound speed is frequency dependent. The modulus from the ultrasonic measurements is significantly higher than from the low frequency measurements and quasi-static torsion experiments [18]. However, the ultrasonic modulus is approximately the same as obtained from the shear wave experiments, see [7, fig. 8], which have similarly high strain rates. Both the high and low strain rate experiments show that the shear modulus decreases with temperature. In addition, the low strain strain experiments show that the shear modulus decreases by three orders of magnitude above the glass transition temperature, 378 K (105 C). It is not known whether the high strain rate modulus displays such a dramatic change. Here our focus is on the microsecond time scale and the glass transition is neglected, *i.e.,* we assume PMMA remains an amorphous solid.

The assumption on $\mathbf{C_p}$ is motivated by metals for which plasticity is due to the motion of dislocations in a crystal. A variation in plastic volume can be associated with a change in porosity, and has been used to describe soils and granular materials. For a polymer the space between molecules (regions of low electron density), often referred to as 'free volume', enters into a model in the same manner as porosity, see *e.g.,* [23]. A decrease in molecular porosity can be associated with an irreversible material change such as a decrease in the polymer chain length or breaking cross links between chains. Modeling this irreversibility is likely to be needed to fit accurately the profile of a release wave behind a shock.

III. UNIAXIAL FLOW EQUATIONS

The flow in shock wave experiments corresponds to uniaxial strain. To compare with shock data, we reduce to a one-dimensional model for uniaxial flow. The deformation gradient for uniaxial strain is

$$\begin{aligned}\mathbf{F} &= \mathbf{diag}[\ V/V_0,\ 1,\ 1\ ] \\ &= \Big(\frac{V}{V_0}\Big)^{1/3} \mathbf{diag}[\ \exp(\tfrac{2}{3}\epsilon),\ \exp(-\tfrac{1}{3}\epsilon),\ \exp(-\tfrac{1}{3}\epsilon)\ ]\ ,\end{aligned}$$

where $\epsilon = \log(V/V_0)$ characterizes the total shear strain. The elastic and plastic right Cauchy-Green tensors have the form

$$\begin{aligned}\mathbf{C} &= \mathbf{diag}[\ \exp(2\epsilon\ ),\ 1,\ 1\ ]\ , \\ \mathbf{C_p} &= \exp\big(-\tfrac{2}{3}\,\epsilon_{\rm pl}\big)\,\mathbf{diag}[\ \exp(2\epsilon_{\rm pl}),\ 1,\ 1\ ]\ ,\end{aligned}$$

where $\epsilon_{\rm pl}$ is a scalar plastic strain variable. The elastic strain tensor is then

$$\begin{aligned}\mathbf{b}_{\rm el} &= \mathsf{J}^{-2/3}\,\mathbf{C_p}^{-1}\mathbf{C} \\ &= \mathbf{diag}[\ \exp(\tfrac{4}{3}\epsilon_{\rm el}),\ \exp(-\tfrac{2}{3}\epsilon_{\rm el}),\ \exp(-\tfrac{2}{3}\epsilon_{\rm el})\ ]\ ,\end{aligned}$$

where $\mathsf{J} = V/V_0 = \exp(\epsilon)$, and

$$\epsilon_{\rm el}(V,\epsilon_{\rm pl}) = \epsilon(V) - \epsilon_{\rm pl} = \log(V/V_0) - \epsilon_{\rm pl}$$

is a scalar elastic shear strain variable.

The 1-D elastic-plastic flow equations are

$$\boxed{\begin{aligned}\frac{\partial}{\partial t}\Big(\rho\Big) + \frac{\partial}{\partial x}\Big(\rho u\Big) &= 0 \\ \frac{\partial}{\partial t}\Big(\rho u\Big) + \frac{\partial}{\partial x}\Big(\rho u^2 - \sigma^{xx}\Big) &= 0 \\ \frac{\partial}{\partial t}\Big(\rho\, E\Big) + \frac{\partial}{\partial x}\Big(\rho E\, u - \sigma^{xx} u\Big) &= 0 \\ \frac{\partial}{\partial t}\Big(\rho\,\epsilon_{\rm pl}\Big) + \frac{\partial}{\partial x}\Big(\rho\, u\,\epsilon_{\rm pl}\Big) &= \rho\,\mathcal{R}_{\rm pl}\end{aligned}} \tag{1}$$

where $E = \frac{1}{2}u^2 + \mathcal{E}$ is the total specific energy, and $\mathcal{R}_{\rm pl}$ is the plastic strain rate. These equations model the conservation laws of mass, momentum and energy with an additional evolutionary equation for the plastic strain variable.

We assume that the energy has the form

$$\mathcal{E}(V,\epsilon_{\rm pl},S) = \mathcal{E}_{\rm hydro}(V,S) + \mathcal{E}_{\rm shear}\big(V,\epsilon_{\rm el}(V,\epsilon_{\rm pl})\big)\ . \tag{2}$$

Then the longitudinal stress can be expressed as

$$\sigma^{xx} = -(P_{\rm hydro} + P_{\rm shear} + P_{\rm dev})\ , \tag{3}$$

where the stress components are

$$\begin{aligned}P_{\rm hydro} &= -\frac{\partial \mathcal{E}_{\rm hydro}}{\partial V}\ , \\ P_{\rm shear} &= -\frac{\partial \mathcal{E}_{\rm shear}}{\partial V}\ , \\ P_{\rm dev} &= -\frac{1}{V}\,\frac{\partial \mathcal{E}_{\rm shear}}{\partial \epsilon_{\rm el}}\ .\end{aligned} \tag{4}$$

The elastic thermodynamic identity reduces to

$$d\mathcal{E} = \sigma^{xx}\,dV + P_{\rm dev}\,d\epsilon_{\rm pl} + T\,dS\ .$$

Hence in 1-D the elastic-plastic equations are the analog of the fluid equations with the fluid pressure replaced by the longitudinal stress plus an internal degree of freedom for the plastic strain which evolves with a rate equation. From the thermodynamic identity for the hydrodynamic component of the energy,

$$d\mathcal{E}_{\rm hydro} = -P_{\rm hydro}\,dV + T\,dS\ ,$$

the hydro component of the pressure can be expressed in terms of energy rather than the entropy,

$$P_{\rm hydro}(V,\epsilon_{\rm el},\mathcal{E}) = P_{\rm hydro}\big(V,\mathcal{E} - \mathcal{E}_{\rm shear}(V,\epsilon_{\rm el})\big)\ .$$

This simplification is possible only when $\mathcal{E}_{\rm shear}$ is independent of T, *i.e.,* the temperature dependence of the shear modulus is neglected.

A. Reduced Constitutive Model

The shear energy for the model in the previous section reduces to

$$\mathcal{E}_{\rm shear}(V,\epsilon_{\rm el}) = \tfrac{1}{2}\,V\,G(V)\,\Big[\exp(\tfrac{4}{3}\epsilon_{\rm el}) + 2\,\exp(-\tfrac{2}{3}\epsilon_{\rm el}) - 3\Big]\ .$$

The components of the stress are then

$$\begin{aligned} P_{\rm shear}(V,\epsilon_{\rm el}) = &\ -\tfrac{1}{2}\frac{d}{dV}\Big[V\,G(V)\Big] \\ &\Big[\exp(\tfrac{4}{3}\epsilon_{\rm el}) + 2\,\exp(-\tfrac{2}{3}\epsilon_{\rm el}) - 3\Big]\ , \\ P_{\rm dev}(V,\epsilon_{\rm el}) = &-\tfrac{2}{3}\,G(V)\,\Big[\exp(\tfrac{4}{3}\epsilon_{\rm el}) - \exp(-\tfrac{2}{3}\epsilon_{\rm el})\Big]\ . \end{aligned}$$

Note that the stress and strain variables (σ^{xx}, $\epsilon_{\rm el}$ and $\epsilon_{\rm pl}$) are positive in tension, while the pressure variables ($P_{\rm hydro}$, $P_{\rm shear}$, $P_{\rm dev}$) are positive in compression. From the acoustic tensor, it can be shown that the longitudinal and transverse acoustic speeds are given by

$$\begin{aligned} \rho\,c_{\rm long}^2 &= V\,\Big(\frac{\partial}{\partial V}\sigma^{xx}\Big)_{\epsilon_{\rm pl},S} \\ &= \rho\,c_{\rm hydro}^2 + \tfrac{4}{3}\rho\,c_{\rm tran}^2 \\ &\quad + \tfrac{2}{9}\big[\exp(\tfrac{4}{3}\epsilon_{\rm el}) - \exp(-\tfrac{2}{3}\epsilon_{\rm el})\big]G \\ &\quad + \big[\tfrac{7}{3}\exp(\tfrac{4}{3}\epsilon_{\rm el}) + \tfrac{2}{3}\exp(-\tfrac{2}{3}\epsilon_{\rm el}) - 3\big]V\frac{d}{dV}G \\ &\quad + \tfrac{1}{2}\big[\exp(\tfrac{4}{3}\epsilon_{\rm el}) + 2\exp(-\tfrac{2}{3}\epsilon_{\rm el}) - 3\big]V^2\frac{d^2}{dV^2}G\ , \end{aligned} \tag{5}$$

$$\rho\,c_{\rm tran}^2 = G(V)\,\exp(\tfrac{4}{3}\epsilon_{\rm el})\ . \tag{6}$$

In the limit of small elastic shear strain, to leading order,

$$\begin{aligned} \mathcal{E}_{\rm shear} &= \tfrac{2}{3}\,V\,G(V)\,\epsilon_{\rm el}^2\ , \\ P_{\rm shear} &= -\tfrac{2}{3}\frac{d}{dV}\Big[V\,G(V)\Big]\,\epsilon_{\rm el}^2\ , \\ P_{\rm dev} &= -\tfrac{4}{3}\,G(V)\,\epsilon_{\rm el}\ , \\ \rho\,c_{\rm long}^2 &= \rho\,c_{\rm hydro}^2 + \tfrac{4}{3}\rho\,c_{\rm tran}^2 + \tfrac{4}{9}\,G(V)\,\epsilon_{\rm el} + \tfrac{8}{3}\,\frac{d\,G}{dV}\,\epsilon_{\rm el}\ , \\ \rho\,c_{\rm tran}^2 &= G(V)\,(1+\tfrac{4}{3}\epsilon_{\rm el})\ . \end{aligned}$$

We note that $\mathcal{E}_{\rm shear}$ and $P_{\rm shear}$ are second order, while $P_{\rm dev}$ is proportional to the shear strain. The standard shear stress model is linear and corresponds to neglecting second order terms. However, we include the non-linear terms because the elastic shear strain may not be small in a shock profile. With the power of computers today, there is no need to employ the simplified linear shear stress model in numerical simulations.

B. Mie-Grüneisen Form

To fit the data for PMMA, it is convenient to use a Mie-Grüneisen form for the stress

$$\begin{aligned} \sigma^{xx}(V,e,\epsilon_{\rm pl}) =& \sigma_h^{xx}(V) - \frac{\Gamma}{V}\big[e - e_h(V)\big] \\ &- \Big(\frac{\partial}{\partial\epsilon_{\rm el}}\sigma^{xx}\Big)_{V,e}\big[\epsilon_{\rm pl} - \epsilon_Y(V)\big]\ , \end{aligned} \tag{7}$$

where Γ is the Grüneisen coefficient, σ_h^{xx}, $e_h = e_0 + \frac{1}{2}(\sigma_h^{xx} - \sigma_0^{xx})\,(V - V_0)$ and ϵ_Y are the longitudinal stress, energy and plastic strain, respectively, on the principal Hugoniot locus.

For the model we are using

$$\begin{aligned} \Big(\frac{\partial}{\partial\epsilon_{\rm el}}\sigma^{xx}\Big)_{V,e} &= -\frac{\partial}{\partial\epsilon_{\rm el}}\Big(P_{\rm shear} + P_{\rm dev}\Big)_V \\ &= \tfrac{4}{3}\rho\,c_{\rm tran}^2 + \tfrac{2}{3}\big[\exp(\tfrac{4}{3}\epsilon_{\rm el}) - \exp(-\tfrac{2}{3}\epsilon_{\rm el})\big] \\ &\qquad \Big[\tfrac{1}{3}G + V\frac{d}{dV}G\Big]\ , \end{aligned} \tag{8}$$

$$\begin{aligned} (\rho\,c_{\rm long})^2 &= \Big(\frac{\partial}{\partial V}\sigma^{xx}\Big)_{e,\epsilon_{\rm pl}} + \Big(\sigma^{xx}\frac{\partial}{\partial e}\sigma^{xx}\Big)_{V,\epsilon_{\rm pl}} \\ &= \frac{d}{dV}\sigma_h^{xx} - \tfrac{1}{2}\frac{\Gamma}{V}\big(V_0 - V\big)\Big[\frac{d}{dV}\sigma_h^{xx} - (\rho_0\,u_s)^2\Big] \\ &\quad + \tfrac{2}{3}\Big\{2\,\rho\,c_{\rm tran}^2 + \big[\exp(\tfrac{4}{3}\epsilon_{\rm el}) - \exp(-\tfrac{2}{3}\epsilon_{\rm el})\big] \\ &\qquad \big[\tfrac{1}{3}G + V\frac{d}{dV}G\big]\Big\}\frac{d}{dV}\epsilon_Y\ , \end{aligned} \tag{9}$$

$$\rho\,c_{\rm tran}^2 = \exp(\tfrac{4}{3}\epsilon_{\rm el})\,G(V)\ , \tag{10}$$

where u_s is the shock speed, and is determined by $(\rho_0\,u_s)^2 = \Delta(\sigma^{xx})/\Delta(V)$.

The Grüneisen coefficient can be determined from temperature measurements along an isentrope using the thermodynamic relation

$$\frac{\partial T}{\partial P}\Big|_S = \frac{T\,\Gamma}{K_s}\ ,$$

where K_s is the isentropic bulk modulus. For hydrostatic compression, Rodriquez and Filisko [15] measured the temperature along several isentropes (by varying the initial temperature at atmospheric pressure) up to a pressure of 0.2 GPa. Though K_s was not measured, in that range the variation should be relatively small. Yet $\Delta T/\Delta P$ varies with temperature by a factor of over 2 [15, fig. 5]. For uniaxial compression, starting at atmospheric pressure and room temperature, Rosenberg & Partom [16] measured the temperature up to 1.6 GPa. From their measurements they obtained $\Gamma/V = 0.765 \pm 0.015$. However, based on Rodriquez and Filisko data, in general Γ depends on both V and T.

Our focus is on the principal shock Hugoniot for which the entropy increases with pressure, and up to a higher pressure (10 GPa) than the measurements from which Γ can be inferred. We assume along the Hugoniot that the Grüneisen coefficient can be expressed in terms of the compression as

$$\Gamma(\eta) = \Gamma_0 + \Gamma_1\eta + \Gamma_2\eta^2 \ ,$$

where $\eta = 1 - V/V_0$. Since weak shocks are nearly isentropic, we take $\Gamma_0 = -\Gamma_1$ in order that Γ/V is constant for small compression, $\eta \ll 1$, and treat Γ_2 as a fitting parameter. For the value of Γ_0 we use the thermodynamic relation

$$\Gamma/V = \beta K_s/C_p \ ,$$

where β is coefficient of volumetric expansion, the bulk modulus is determined from the acoustic speeds $K_s = \rho\,(c_{\rm long}^2 - \frac{4}{3}c_{\rm tran}^2)$ and C_p is specific heat at constant pressure. At the initial state, $\rho = 1.185\,{\rm g/cm^3}$, the coefficient of linear expansion[3] is $\beta/3 = 63 \times 10^{-6}/{\rm K}$, $C_p = 1.38 \times 10^{-3}\,{\rm MJ\,(kg\,K)^{-1}}$, $c_{\rm long} = 2.75\,{\rm km/s}$ and $c_{\rm tran} = 1.4\,{\rm km/s}$. This yields $\Gamma_0 = 0.7$ which is slightly larger than the value obtained by Rosenberg & Partom.

By subtracting the shear stress and shear energy components, the principal Hugoniot locus determines a reference curve for the hydrostatic component of the equation of state. Along the hydrostatic reference curve the temperature is determined by integrating the ODE

$$\frac{d}{dV}T_{\rm ref}(V) + \frac{\Gamma}{V}T_{\rm ref}(V) = \Big[P_{\rm ref}(V) + \frac{d}{dV}e_{\rm ref}(V)\Big]C_v^{-1} \ ,$$

where C_v is the specific heat at constant V. It is thermodynamically consistent with Γ a function of only V to take the specific heat to be a constant. For a constant specific heat, the temperature is given by

$$T(V,\epsilon_{\rm el},\mathcal{E}) = T_{\rm ref}(V) + \big[\mathcal{E} - \mathcal{E}_{\rm shear}(V,\epsilon_{\rm el}) - e_{\rm ref}(V)\big]/C_v \ .$$

Due to the excitation of molecular vibrations, the specific heat at constant pressure increases from $1.39\,{\rm J/(g\,K)}$ at $300\,{\rm K}$ to $2.44\,{\rm J/(g\,K)}$ at $550\,{\rm K}$ [14, table 4]. Here we use the value at the glass transition temperature $378\,{\rm K}$, $C_p = 1.7\,{\rm J/(g\,K)}$ which will overestimate the temperature on the Hugoniot at high pressure. This corresponds to $C_v = \frac{C_p}{1+\beta\,T\,\Gamma} = 1.64 \times 10^{-3}\,{\rm MJ\,(kg\,K)^{-1}}$. In general the V and T dependence of the specific heat and the Grüneisen coefficient are related. Accounting for the temperature dependence more accurately is beyond the scope of this paper.

[3] From `http://www.dow.com/styron/design/guide/thermal.htm`

C. Plastic Strain Rate

We assume that the plastic strain rate has the form

$$\mathcal{R}_{\rm pl}(V,\epsilon_{\rm el}) = \tfrac{1}{2}\,\frac{\max(\tilde{\rm Y} - Y, 0)}{\mu}{\sf sgn}(\epsilon_{\rm el}) \ ,$$

where $\tilde{\rm Y}({\sf dev}\,\boldsymbol{\sigma})$ is the yield function, Y is the yield strength and μ is a parameter with dimensions of viscosity (pressure×time) that controls the relaxation rate of the shear stress to the yield surface. For an isotropic material, such as a polymer, it is reasonable to use the Von Mises yield function, $\tilde{\rm Y} = \sqrt{3/2}\,\|{\sf dev}\,\boldsymbol{\sigma}\|$. For uniaxial flow, the Von Mises yield function reduces to

$$\tilde{\rm Y}(V,\epsilon_{\rm el}) = \tfrac{3}{2}\,|P_{\rm dev}| = G(V)\,|\exp(2\epsilon_{\rm el}) - 1|\exp(-\tfrac{2}{3}\epsilon_{\rm el}) \ .$$

We further assume that the yield strength is a function of V. Based on the available data for PMMA, it is convenient to specify the plastic strain on the yield surface, $\epsilon_{\rm pl} = \epsilon_Y(V)$, and define the yield strength by, $Y(V) = \tilde{\rm Y}(V, \log(V/V_0) - \epsilon_Y(V))$.

We note that in the limit of slow strain rates, $|(d/dt)\epsilon| = |\nabla\cdot\vec{u}| \ll Y/\mu$, the plastic flow regime reduces to rate-independent plasticity with an additional viscous stress

$$\boldsymbol{\sigma}_{\rm vis} = \mu\left[\nabla\otimes\vec{u} + (\nabla\otimes\vec{u})^\dagger\right] \ .$$

Moreover, with $Y = 0$, the elastic-plastic model reduces to a visco-elastic model.

With the yield strength defined in terms of ϵ_Y, the plastic strain rate can be re-expressed as

$$\mathcal{R}_{\rm pl}(V,\epsilon_{\rm el}) = \frac{\max(|\epsilon_{\rm pl} - \epsilon_Y|, 0)}{\tau}{\sf sgn}(\epsilon_{\rm el}) \ ,$$

where τ is a relaxation time constant. To fit wave profiles, the relaxation time constant needs to decrease with the distance from yield surface. We assume that τ can be fit with the form

$$\tau = \tau_0(V)\left(1 + \Big[\frac{|\epsilon_{\rm pl} - \epsilon_Y|}{\epsilon_0}\Big]^n\right)^{-1} \ , \qquad (11)$$

where ϵ_0 and n are parameters, and $\tau_0(V)$ is the time constant at the yield surface.

We note that the time constant and the viscous parameter are related by

$$\tau_0(V) = \tfrac{4}{3}\,\frac{\mu_0(V)}{-\frac{\partial}{\partial\epsilon_{\rm el}}P_{\rm dev}} \ .$$

In the limit of small elastic strain, $\tau_0(V) = \frac{\mu_0(V)}{G(V)}$. Moreover, the dependence of τ on $\epsilon_{\rm pl} - \epsilon_Y$ is analogous in a visco-elastic model to μ depending on $(d/dt)\epsilon$ since the distance from the yield surface increases with strain rate.

Substituting Eq. (11) into the plastic strain rate equation yields

$$\frac{d}{dt}\epsilon_{\rm pl} = -\frac{(\epsilon_{\rm pl} - \epsilon_Y)\Big(1 + [(\epsilon_{\rm pl} - \epsilon_Y)/\epsilon_0]^n\Big)}{\tau_0(V)} \ , \qquad (12)$$

for $\epsilon_Y(V) \le \epsilon_{\rm pl} \le 0$. Many hyperbolic PDE solvers account for source terms with an operator split algorithm. Holding V fixed the solution to Eq. (12) is

$$\epsilon_{\rm pl}(t+\Delta t) = \epsilon_Y + \frac{[\epsilon_{\rm pl}(t)-\epsilon_Y]\exp(-\Delta t/\tau_0)}{\left\{1+\left[\frac{\epsilon_{\rm pl}(t)-\epsilon_Y}{\epsilon_0}\right]^n\left[1-\exp(-n\Delta t/\tau_0)\right]\right\}^{1/n}} \ . \quad (13)$$

Consequently, the source term for the plastic strain can be accounted for efficiently.

IV. FITTING PARAMETERS

Experimental data for PMMA are used to calibrate parameters in a Mie-Grüneisen equation of state. The data are parameterized by the compression ratio $\eta = 1 - V/V_0$. Measurements of the shock Hugoniot, fit by Schuler & Nunziato [6], determine σ_h^{xx}. Schuler & Nunziato also measured and fit the release wave speed which determines the longitudinal sound speed behind the shock. Static measurements of the transverse sound speed up to to 1 GPa [3] were used to constrain the fit of the shear modulus.

Given σ_h^{xx} and $c_{\rm long}$ from experiments and assuming that $G(V)$ and $\Gamma(V)$ are known, Eq. (9) determines $(d/dV)\epsilon_Y$, which can be integrated to determine the plastic strain on the yield surface as a function of V. This in turn determines the shear stress behind the shock front. Measurements of the shear stress [12] were used to constrain the shear modulus at stresses above the static measurements and the quadratic coefficient of Γ. The parameters were varied to obtain a reasonable fit. The values of the parameters are listed in tables 1-4.

Data and fits for the shock velocity and acoustic speeds along the Hugoniot locus are shown in figure 1. The fit to the shear stress is shown in figure 2. The total, elastic and plastic strains are shown in figure 3. By taking the yield strength to be a function of V, the shock velocity is monotonically increasing with stress and an elastic precursor does not occur. We note that the equilibrium elastic shear strain is about a factor of ten larger than is typical for metals. The bulk and shear moduli are shown in figure 4. The difference between the hydrostatic and uniaxial bulk modulus is dominated by the $(d/dV)G$ term in Eq. (5).

The change in slopes of shock velocity in figure 1, of shear stress in figure 2, of elastic strain in figure 3 and of the hydrostatic bulk modulus in figure 4, all correspond to the same compression. Very likely shock compression causes bonds in the polymer chain to break, and the chains to pack together more closely. This is compatible with a decrease in porosity lowering the rate of increase of the hydrostatic sound speed with compression. Model possibly could use the plastic volume to account for such an irreversible change. One would expect the release wave profile to be affected by a change in plastic volume.

The equation of state determines the Hugoniot loci. Two loci are of importance. The frozen locus holds the plastic strain fixed while for the equilibrium locus the plastic strain is determined by the yield surface. Both loci are shown in figure 5 for the principal Hugoniot. It

TABLE I: Fit to stress on principal Hugoniot [6, Eq. (3.8) and footnote 5], parameterized by $\eta = 1 - V/V_0$.

$\sigma_h^{xx}(\eta) = \eta \sum a_i \eta^i$	
a_0	8.979 GPa
a_1	70.0
a_2	-586.9
a_3	1965.2

TABLE II: Fit to Lagrangian longitudinal sound speed on principal Hugoniot [6, Eq. (3.9) and footnote 6], parameterized by $\eta = 1 - V/V_0$.

$\rho_0\,[\rho\, c_{\rm long}(\eta)/\rho_0]^2 = \sum b_i \eta^i$	
b_0	9.031 GPa
b_1	141.4
b_2	-677.9
b_3	4160.0

TABLE III: Hydrostatic shear modulus fit to transverse sound speed data [3], parameterized by $\eta = 1 - V/V_0$.

$G(\eta) = \sum G_i \eta^i$	
G_0	2.31 GPa
G_1	15.
G_2	80.

TABLE IV: Grüneisen coefficient parameterized by $\eta = 1 - V/V_0$.

$\Gamma(\eta) = \sum \Gamma_i \eta^i$	
Γ_0	0.7
Γ_1	-0.7
Γ_2	8.

TABLE V: Plastic strain rate parameters.

τ_0	0.2	μs
ϵ_0	0.025	
n	4	

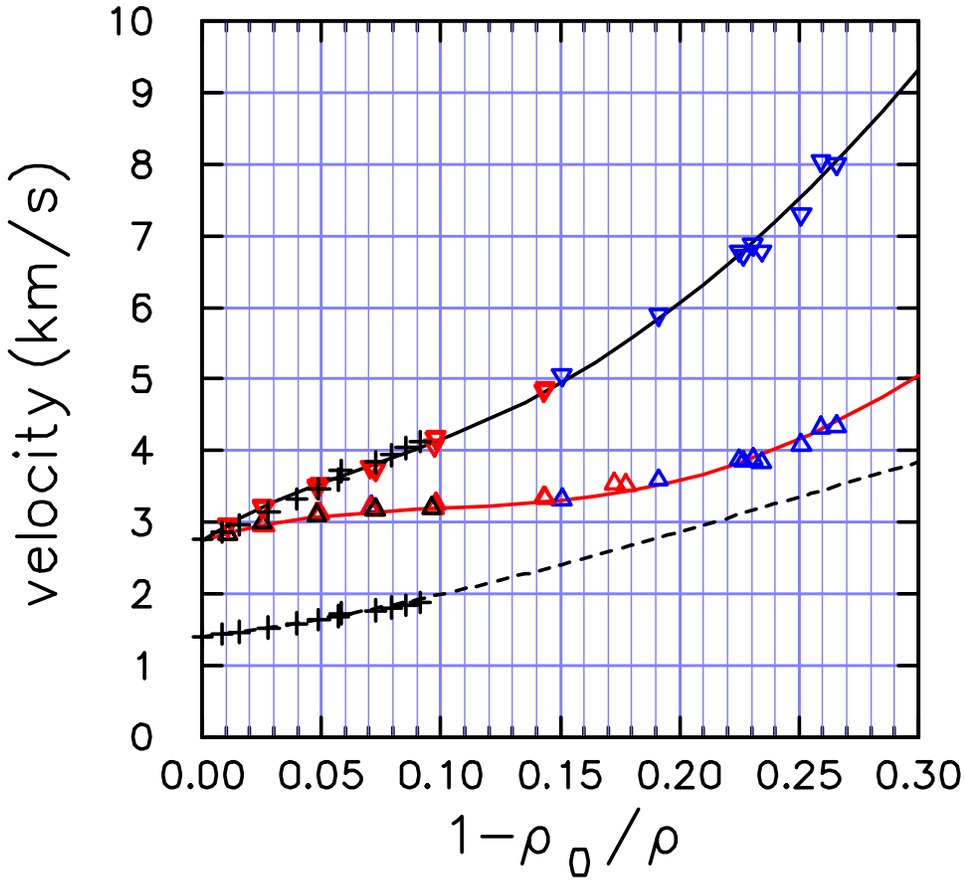

FIG. 1: Wave speeds as a function of compression. Red and black curves correspond to shock speed and Lagrangian longitudinal sound speed behind shock, respectively. Red, blue and black triangles are the data from Barker & Hollenbach [5], Schuler & Nunziato [6] and Schuler [4], respectively. The dashed black curve is the Lagrangian transverse sound speed, and the plus symbols are the static data of Stephens, Heard & Schock [3].

follows from these loci that the wave profile for any shock wave is partly dispersed; a frozen shock followed by a relaxation layer to point on the equilibrium locus with the same shock velocity. In particular, a result of the yield strength increasing with compression is that the equilibrium shock velocity is strictly monotonically increasing, and consequently an elastic precursor does not occur.

The estimated shock temperature is shown in figure 6. At high pressures the shock temperature is considerably higher than the glass transition temperature at atmospheric pressure, 378 K. Whether a shock causes melting depends on how much the transition temperature increases with pressure and on the time scale for the transition. The measured shear stress shown in figure 2 indicates that up to at least 4 GPa the shear modulus has not changed dramatically, hence, melting has not occured. Furthermore, the change in slope of the shear stress occurs below 2 GPa and the temperature is below the glass transition temperature at atmospheric pressure. The same is true for the slope change of shock velocity shown in figure 1. Thus the change in slope of the Hugoniot is not due to melting. Instead the Hugoniot is affected by the change in the elastic strain shown in figure 3, *i.e.,* plastic yield phenomena.

V. WAVE PROFILES

Measurements of shock wave profiles by Barker & Hollenbach [5] and Schuler & Nunziato [6] are used to calibrate the plastic strain rate for PMMA. Strain rate parameters are adjusted until simulated VISAR data compares favorably with the experimental records; in particular, figure 3 of [6]. Admittedly this is a crude approach. But electronic data files for the wave profiles are not available since the experiments were performed in the 1970s before the advent of PCs and the Internet. Unfortunately, there is still no mechanism within the high pressure research community for obtaining data electronically.

Simulations of piston driven waves were performed using an adaptive mesh Lagrangian algorithm (second order Godunov scheme) within the Amrita environment of James Quirk [24–26]. The rate parameters used are listed

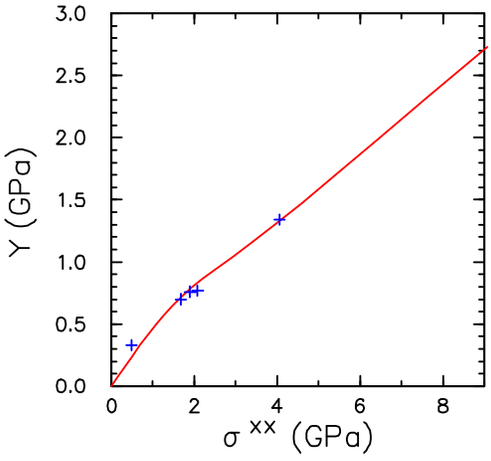

FIG. 2: Shear stress as a function of longitudinal stress on Hugoniot locus. $Y = \frac{3}{2}\,\|\mathsf{dev}\,\sigma\| = \sigma^{xx} - \sigma^{yy}$. Red curve is from model and symbols are data from Millett & Bourne [12].

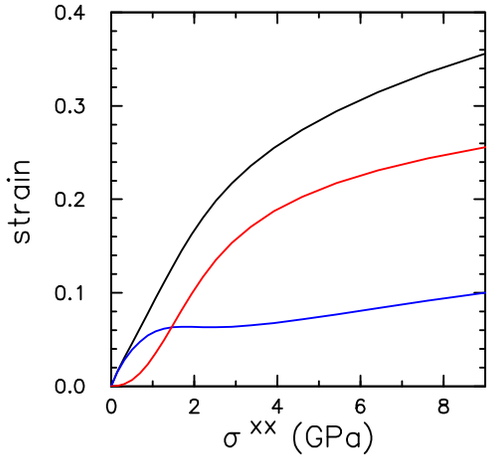

FIG. 3: Strain as a function of longitudinal stress on Hugoniot locus. Black, blue and red curves correspond to total strain, $\epsilon = \log(\rho/\rho_0)$, elastic strain, $\epsilon_{\rm el} = \epsilon - \epsilon_{\rm pl}$, plastic strain, $\epsilon_{\rm pl}$, respectively.

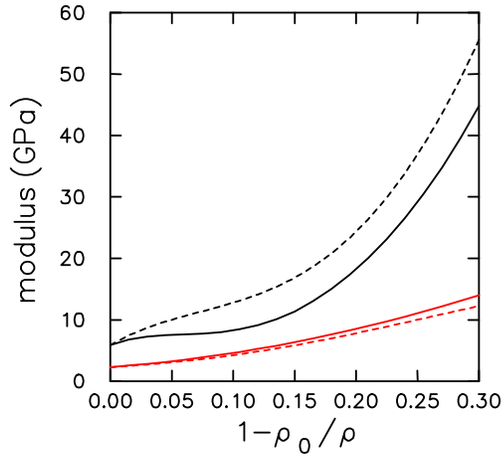

FIG. 4: Moduli vs. compression. Black and red curves are the bulk and shear moduli, respectively, based on the acoustic speeds; $K = \rho\,(c^2_{\rm long} - \frac{4}{3}c^2_{\rm tran})$ and $G = \rho\,c^2_{\rm tran}$. The solid and dashed curves represent hydrostatic and uniaxial shock compression, respectively. The acoustic speeds along the shock Hugoniot are given by Eqs. (9) and (10) with $\epsilon_{\rm el} = \log(V/V_0) - \epsilon_Y(V)$, and the hydrostatic acoustic speeds from Eqs. (5) and (6) with $\epsilon_{\rm el} = 0$.

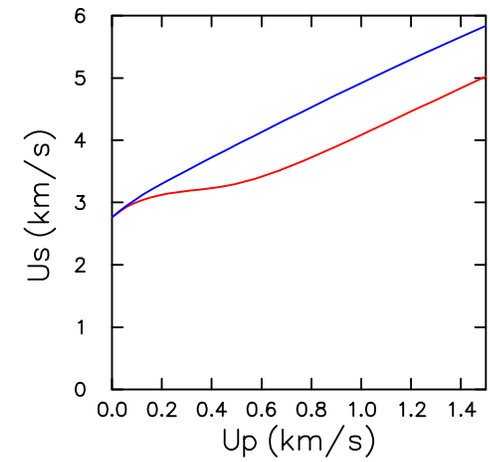

FIG. 5: Shock Hugoniot in (particle velocity, shock velocity)–plane. Blue and red curves are frozen and equilibrium loci, respectively.

in table V. The results for three case are shown in figure 7. The simulated VISAR records are the particle velocity along a Lagrangian particle path for a sequence of positions, and the wave profiles are of the elastic shear strain at a sequence of times.

The three cases are distinguished by the shock strength. Their salient features are as follows:

1. Weak shock; piston velocity 0.08 km/s and longitudinal stress 0.28 GPa
   The VISAR profiles are dominated by the frozen shock with a small particle velocity change in the relaxation layer. The elastic shear strain varies monotonically.

2. Medium shock; piston velocity 0.3 km/s and longitudinal stress 1.1 GPa
   The sequence of VISAR records clearly shows that the particle velocity behind the frozen shock decreases with distance of run towards its asymptotic value given by the frozen Hugoniot locus. There is a larger velocity change in the relaxation layer than for a weaker shock. The elastic shear strain overshoots and than relaxes to the value corresponding to the equilibrium Hugoniot locus.

3. Strong shock; piston velocity 1.1 km/s and longitu-

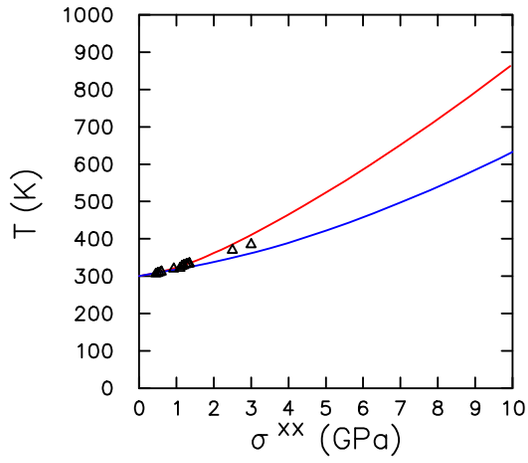

FIG. 6: Estimated shock temperature vs. longitudinal stress. Blue and red curves are frozen and equilibrium loci, respectively. Symbols are data from Rosenberg & Partom [17]. The temperatures above 378 K are high due to the use of a constant specific heat.

dinal stress 5.6 GPa

The apparent particle velocity behind the frozen shock front, both experiment [6, fig. 3b] and simulation, is substantially larger than for the frozen Hugoniot shown in figure 5. This is a consequence of the shear stress behind the frozen shock being far from the yield surface resulting in a very small relaxation time constant. This is evident in the spike of the elastic shear strain immediately behind the frozen shock front. Typically VISAR experiments have a temporal resolution of about 1 ns. On this time scale, the discontinuity of the frozen shock is not distinguishable from the very large slope caused by the fast decrease in the elastic shear strain immediately behind the shock front. Since the relaxation time constant increases as the shear stress approaches the yield surface, only a small rollover in the velocity profile is observed.

For the strong shock case, a few comments on the numerics are in order. To calculate the spike in the elastic shear strain efficiently, an adaptive mesh algorithm is needed. The simulations here used an initial cell size of 50 μm, and 3 levels of refinement by a factor of 4. Hence the effective resolution is 0.78 μm. In addition, it is important to integrate accurately the source term for the plastic strain, Eq. (12). A form for the plastic strain rate that lends itself to evaluating the integral exactly, such as Eq. (13), or at least an asymptotic expression is advantageous since it avoids having the time step dominated by a stiff source term.

The stability of solutions to the fluid flow equations, hence any numerical algorithm, is dependent on dissipation. Thermodynamic consistency is necessary in order to base dissipation on the physical entropy. The elastic shear strain behind a strong frozen shock is large enough to be outside the domain of linear elasticity. Consequently, to calculate a shock wave profile, it is important for numerical stability to account adequately for the nonlinearities in the constitutive model. This is the reason why we have taken the trouble to present the formalism for a fully nonlinear thermodynamically consistent elastic-plastic model.

The part of the model that has the weakest physical justification is the plastic strain rate. Empirically, this could be improved by including release wave profile data in the calibration. Model development would be facilitated if there were a means to obtain electronically profile data for experiments that have been reported in the literature.

Finally, we would like to emphasis the importance of having a constitutive model that covers a wide range. VISAR records for shock wave profiles of a solid typically display an elastic precursor followed by a plastic wave. For a PMMA window, the precursor can be in the weak to medium shock range in which the frozen Hugoniot dominates the impedance match. In contrast, the plastic wave can be in the strong shock range in which the equilibrium Hugoniot dominates the impedance match. The rate dependent elastic-plastic model covers both regions. In effect, it allows one to interpolate between the frozen and equilibrium response.

[1] L. M. Barker. The development of the VISAR, and its use in shock compression science. In *Shock Compression of Condensed Matter – 1999, Proceedings of the American Physical Society Topical Group on Shock Compression of Condensed Matter, Snowbird, UT*, pages 11–17. American Institute of Physics, NY, 1999.

[2] J. R. Asay, D. L. Lamberson, and Guenther A. H. Pressure and temperature dependence of the acoustic velocities in polymethylmethacrylate. *J. Appl. Phys.*, 40:1768–1783, 1969.

[3] D. R. Stephens, H. C. Heard, and R. N. Schock. High-pressure mechanical properties of PMMA. Technical Report UCID-16007, Lawrence Livermore Laboratory, March 1972.

[4] K. W. Schuler. Propagation of steady waves in PMMA. *J. Mech. Phys. Solids*, 18:277–293, 1970.

[5] L. M. Barker and R. E. Hollenbach. Shock-wave studies of PMMA, fused silica and sapphire. *J. Appl. Phys.*, 41:4208–4226, 1970.

[6] K. W. Schuler and J. W. Nunziato. The dynamic mechanical behavior of polymethyl methacrylate. *Rheol. Acta*, 13:265–273, 1974.

[7] Y. M. Gupta. Determination of the impact response of PMMA using combined compression and shear loading. *J. Appl. Phys.*, 51:5352–5361, 1980.

[8] P. F. Chartagnac. Determination of mean and deviatoric

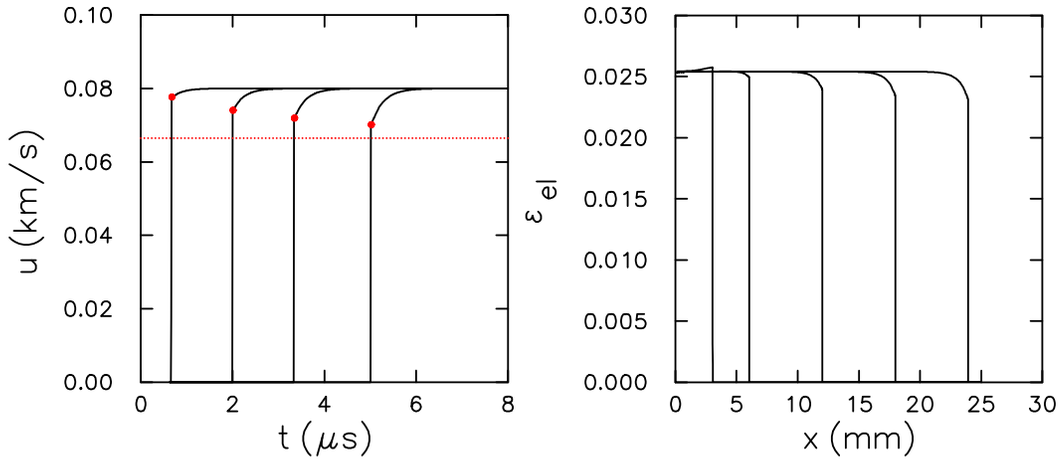

Case 1: weak shock, $u_p = 0.08\,\mathrm{km/s}$ and $\sigma^{xx} = 0.28\,\mathrm{GPa}$

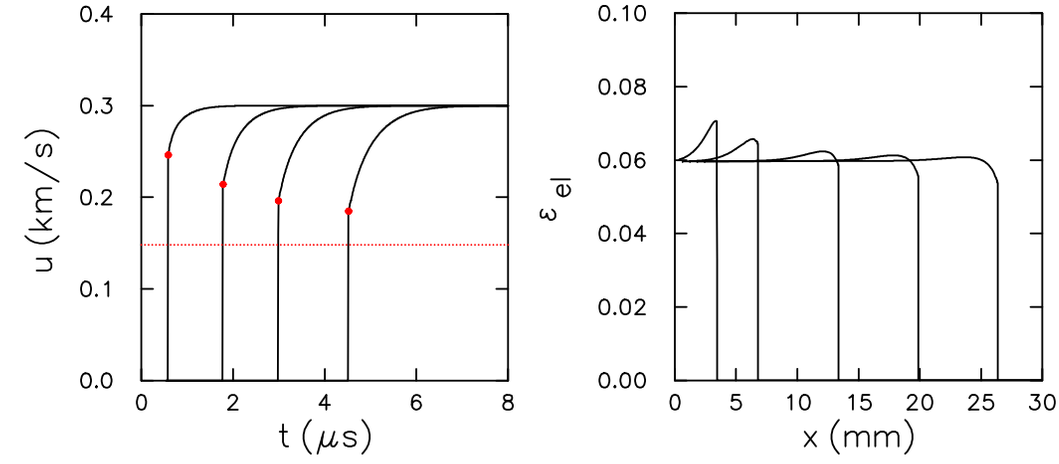

Case 2: moderate shock, $u_p = 0.3\,\mathrm{km/s}$ and $\sigma^{xx} = 1.1\,\mathrm{GPa}$

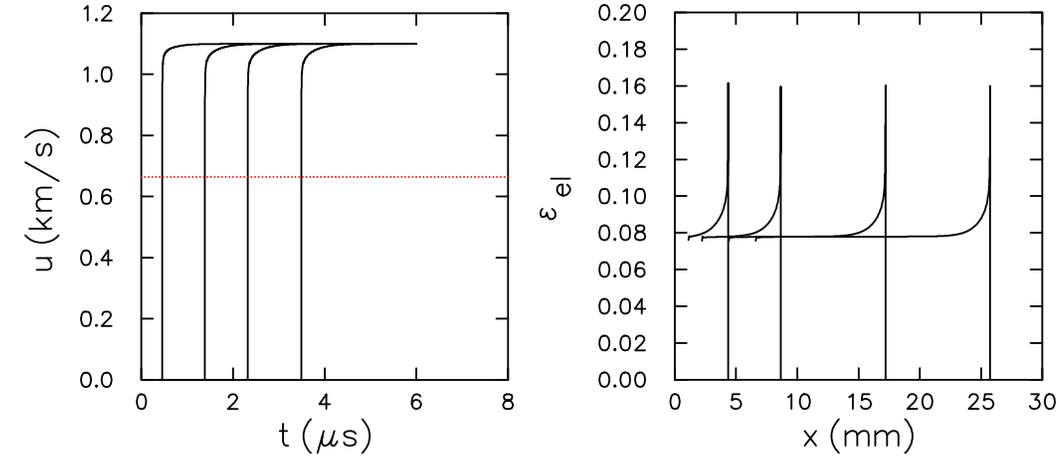

Case 3: strong shock, $u_p = 1.1\,\mathrm{km/s}$ and $\sigma^{xx} = 5.6\,\mathrm{GPa}$

FIG. 7: Simulated VISAR records ($x_0 = 2, 6, 10, 15\,\mathrm{mm}$), and wave profiles ($t = 1, 2, 4, 6, 8\,\mu\mathrm{s}$) of elastic shear strain. Red dots indicate lead shock. Dotted red line is asymptotic (steady state) velocity behind lead shock based on frozen shock locus.

stress in shock loaded solids. *J. Appl. Phys.*, 53:948–953, 1982.

[9] S. C. Gupta and Y. M. Gupta. Piezoresistance response of longitudinally and laterally oriented ytterbium foils subjected to impact and quasi-static loading. *J. Appl. Phys.*, 57:2464–2473, 1985.

[10] Yu. V. Bat'kov, S. A. Novikov, and N. D. Fishman. Shear stresses in polymers under shock compression. In S. C. Schmidt and W. C. Tao, editors, *Shock Compression of Condensed Matter – 1995*, pages 577–580. APS Topical Group on SCCM, AIP, 1996.

[11] N. K. Bourne and Z. Rosenberg. Manganin gauge and VISAR histories in shock-stressed PMMA. *Proc. R. Soc. London A*, 455:1259–1266, 1999.

[12] J. C. Millett and N. K. Bourne. The deviatoric response of PMMA to one-dimensional shock loading. *J. Appl. Phys.*, 88:7037–7040, 2000.

[13] J. Heijboer. Mechanical properties and molecular structure of organic polymers. In J. A. Prins, editor, *Physics of Non-Crystalline Solids*, pages 231–254. North-Holland, 1965.

[14] H. S. Bu, W. Aycock, and B. Wunderlich. Heat capacities of solid, branched macromolecules. *Polymer*, 28:1165–1176, 1987.

[15] E. L. Rodriquez and F. E. Filisko. Thermoelastic temperature changes in poly(methyl methacrylate) at high hydrostatic pressure: Experimental. *J. Appl. Phys.*, 53:6536–6540, 1982.

[16] Z. Rosenberg and Y. Partom. One-dimensional isentropic compression measuremnts of multiply loaded polymethylmethacrylate. *J. Appl. Phys.*, 41:921–923, 1982.

[17] Z. Rosenberg and Y. Partom. Direct measurements of temperature in shock-loaded polymethylmethacrylate with very thin copper thermistors. *J. Appl. Phys.*, 56:1921–1926, 1984.

[18] S. Rabinowitz, I. M. Ward, and J. S. C. Parry. The effect of hydrostatic pressure on shear yield behavior of polymers. *J. Mat Sci.*, 5:29–39, 1970.

[19] R. A. Duckett, S. Rabinowitz, and I. M. Ward. The strain-rate, temperature and pressure dependence of yield of isotropic poly(methylmethacrylate) and poly(ethylene terephthalate). *J. Mat Sci.*, 5:909–915, 1970.

[20] M. C. Boyce, D. M. Parks, and A. S. Argon. Large inelastic deformation of glassy polymers. Part I: Rate dependent constitutive model. *Mechanics of Materials*, 7:15–33, 1988.

[21] Z. Rosenberg and Y. Partom. Accounting for the Hugoniot elastic limit of polymers by using pressure dependent yield criterion. *J. Appl. Phys.*, 76:1935–1936, 1994.

[22] B. J. Plohr and J. N. Plohr. title ? *in preparation*, page ?, 2004.

[23] R. Menikoff and E. Kober. Equation of state and Hugoniot locus for porous materials: P–α model revisited. In *Shock Compression in Condensed Matter–1999*, pages 129–132, 1999.

[24] J. J. Quirk. Amrita - a computational facility for CFD modelling. In *29^{th} Computational Fluid Dynamics*, VKI Lecture Series, chapter 4. von Karmen Institute, 1998. `http://www.galcit.caltech.edu/~jjq/vki/vki:cfd29::jjq_l1.ps.gz`.

[25] J. J. Quirk. AMR_sol: Design principles and practice. In *29^{th} Computational Fluid Dynamics*, VKI Lecture Series, chapter 5. von Karmen Institute, 1998. `http://www.galcit.caltech.edu/~jjq/vki/vki:cfd29::jjq_l2.ps.gz`.

[26] R. Menikoff and J. J. Quirk. Versatile user-friendly EOS package. Technical Report LA-UR-01-6222, Los Alamos National Laboratory, 2001. `http://t14web.lanl.gov/Staff/rsm/preprints.html#EOSpackage`.